Analyzing power measurements in pion-deuteron breakup at intermediate energies

D. M. Yeomans,* E. L. Mathie, G. M. Huber, G. J. Lolos, S. I. H. Naqvi, and V. Pafilis
Department of Physics, University of Regina, Regina, Saskatchewan, Canada S4S 0A2

G. Jones, M. Sevior,† R. P. Trelle,‡ and P. Weber§
Department of Physics, University of British Columbia, Vancouver, British Columbia, Canada V6T 1Z1

R. Tacik, D. Healey, D. F. Ottewell, G. R. Smith, and G. Wait
TRIUMF, Vancouver, British Columbia, Canada V6T 2A3

H. Garcilazo
Escuela Superior de Fisica y Matematicas, Instituto Politechnico Nacional, Edificio 9, 07738 Mexico D.F., Mexico

D. L. Humphrey
Western Kentucky University, Bowling Green, Kentucky 42101
(Received 11 July 1995)

As part of an experimental study of the πNN system, the pion-deuteron breakup reaction $\pi^+\vec{d}\rightarrow pn\pi^+$ was investigated at intermediate energies. Distributions of the vector analyzing power iT_{11} versus outgoing proton momentum P_p are presented for 36 πp angle pairs in the range of scattering angles $20°\leq\theta_p\leq 51°$, $62°\leq\theta_\pi\leq 124°$ at 228 and 134 MeV. These include 7 previously unmeasured angle pairs at 228 MeV and 20 new pairs at 134 MeV. In all regions of overlap with previous measurements, there is excellent agreement. There is generally excellent agreement with relativistic Faddeev predictions, except in the np final-state interaction region at 228 MeV. This is in contrast to the cross-section measurements, which are not well described by the theory.

PACS number(s): 25.10.+s, 24.70.+s, 13.75.−n

I. INTRODUCTION

The study of the pion-deuteron reaction allows us to learn about both pion-nucleon and pion-nuclear interactions [1–3]. Special theoretical techniques are available for treating the dynamics of three-body systems, such as the πNN system. The three-body approach offers the possibility to treat the coupled channels, $NN\rightarrow NN$, $\pi[NN]\rightarrow\pi[NN]$, and $\pi[NN]\leftrightarrow NN$, within a unified and consistent framework. ($[NN]$ represents either the deuteron or NN continuum states.) The strong coupling between the channels helps to ensure that a good theoretical description in any one of the channels is not simply fortuitous. For a stringent test, therefore, the comparison between theory and experiment must be extended to data from as many reaction channels as possible.

Of the inelastic πd channels, by far the largest one in the resonance region ($100<T_\pi<300$ MeV) is the breakup reaction $\pi d\rightarrow pn\pi$ (it is even larger than the elastic one by roughly a factor of 2). Its three-body final state enables systematic studies within one channel across a broad kinematical range. It is thus important to use this reaction as a test of the available theories.

The dominant mechanism by which πd breakup occurs is the single scattering process [4]. Here, the pion interacts with one of the nucleons, which is knocked out of the loosely bound deuteron. The other (spectator) nucleon becomes free and continues to move with the same Fermi momentum that it had at the instant of the collision. In the simple impulse approximation (IA), the amplitude for this process is proportional to $\Phi_d(\mathbf{q})$, the deuteron wave function in momentum space, where $\mathbf{q}$ is the relative momentum of the two nucleons inside the deuteron at the instant of collision. The wave function $\Phi_d(\mathbf{q})$ peaks sharply at $\mathbf{q}=0$. Since $\mathbf{q}$ is equal to the final momentum of the spectator nucleon in the rest frame of the deuteron, i.e., the lab frame, the cross section is large if the momentum of the spectator nucleon in this frame is small. This is referred to as quasifree (QF) scattering. The case where $\mathbf{q}=0$ is called the quasifree point.

If the momentum of the "spectator" nucleon is large in comparison to the deuteron Fermi momentum (say >50 MeV/c), then higher order processes such as πN final state interactions (FSI) (π double scattering) and NN FSI (N double scattering) come into play. At the energies of the resonance region, many processes contribute and the interference can lead to significant effects. For example, the addition of the rescattering terms can reduce the simple impulse approximation cross section by about 25% [5]. In general, QF πp scattering occurs if the outgoing neutron momentum, p_n, is small; πp FSI occur at large p_n; np FSI occur if the relative momentum between the outgoing neutron and proton is small. In addition, more complicated reaction dynamics may occur in kinematical regions where the principal diagrams no longer dominate.

*Present address: Golder Associates, Nottingham, NG12 4DG England.
†Present address: University of Melbourne, Victoria, Australia.
‡Present address: Chemische Werke Bayer, Leverkusen, Germany.
§Present address: E.T.H., Zurich, Switzerland.

Since there are relatively few measurements for reaction channels with three outgoing particles, the comparison between theory and experiment for the $\pi d \rightarrow \pi NN$ channel should still be made exclusively on the basis of each observable (as opposed to, for example, through helicity amplitudes) [4]. A comprehensive review of these measurements up to 1990 has been published by Garcilazo and Mizutani [4]. To distinguish between various theoretical predictions, an investigation of phase space far from quasifree kinematics is required. There, the cross-section is small, resulting in large statistical errors. In the region of np FSI, iT_{11} is particularly sensitive to the details of different models. This region corresponds to large angle πd elastic scattering, where all theories have well established difficulties describing cross section, vector analyzing power, and tensor observables above $T_\pi = 180$ MeV.

To address these issues, an experimental program was begun at the M11 medium energy pion channel at TRIUMF. The purpose of the experiments was to increase the phase space coverage whilst providing some overlap with previous measurements, and to reduce statistical uncertainties. Systematic uncertainties in iT_{11} measurements were reduced in part through high target polarizations. Triple differential cross sections were measured for $\pi^+ d \rightarrow pn\pi^+$ for 36 angle pairs at 228 MeV using a time-of-flight (TOF) spectrometer and compared with a three-body Faddeev calculation by Garcilazo [6]. Agreement is quite good at most angles, while appreciable deviations are observed for some angle pairs. The vector analyzing power, iT_{11}, was also measured for 36 πp scattering angle pairs spanning the range $20° < \theta_p < 51°$, $62° < \theta_\pi < 124°$ at 134, 180, and 228 MeV in a separate experiment, which is described in this paper.

II. EXPERIMENTAL TECHNIQUE

A. Formalism

The formalism has been described previously [7]. For the setup of the TOF spectrometer as used in this experiment (described below), the vector analyzing power, iT_{11}, is given by

$$iT_{11} = -\frac{(1-X)}{\sqrt{3}P_z}\left(\frac{\sigma_+ - \sigma_-}{\sigma_+ + \sigma_-}\right), \tag{2.1}$$

where P_z is the average magnitude of the target vector polarization, σ_+ is the differential cross section measured for $P_z > 0$, σ_- is the corresponding cross section for $P_z < 0$, and

$$X = \frac{P_{zz}}{2}\left(\frac{T_{20}}{\sqrt{2}} + \sqrt{3}T_{22}\right). \tag{2.2}$$

Here P_{zz} is the target tensor polarization, and T_{kq} are the analyzing powers. All quantities are defined consistent with the Madison convention [8]. For a typical value, $P_z = 0.30$, the maximum possible value of X is 0.086. Based upon comparisons of the average of the polarized cross sections compared to those determined from the same target in an unpolarized state, this term was not significant and has been neglected. For the case where $P_z^+ \neq P_z^-$, and the experimental background is considered, the iT_{11} is given by

$$iT_{11} = -\frac{1}{\sqrt{3}}\left[\frac{\sigma_+ - \sigma_-}{P_z^-\sigma_+ + P_z^+\sigma_- - \sigma_b(P_z^+ + P_z^-)}\right]. \tag{2.3}$$

The background cross section, σ_b, was measured separately with a special target.

Since there are three particles in the final state, there is a distribution of proton momenta for a given πp angle pair coincidence. The cross sections appearing in Eq. (2.3) are symbols for the relative differential cross sections:

$$\frac{d^3\sigma}{d\Omega_\pi d\Omega_p dP_p} = \frac{\text{Yield} \times S_\pi}{N_{\text{beam}} N_{\text{tgt}} \Delta\Omega_\pi \Delta\Omega_p \Delta P_p \, \epsilon \, \epsilon_\pi \, \epsilon_p}, \tag{2.4}$$

where, "Yield" is the number of events, S_π is the correction for fraction of beam bursts with two pions, N_{beam} is the number of incident beam particles, N_{tgt} is the areal density of deuterons, $\Delta\Omega_\pi, \Delta\Omega_p$ are the pion and proton telescope solid angles, ΔP_p is the proton momentum bite, ϵ is the lifetime of data acquisition system, and ϵ_π, ϵ_p are the pion and proton detection efficiencies.

The proton momentum, P_p, is determined from the measured TOF, as discussed below. For a particular path length, L, and total energy, E, the momentum bite, ΔP_p, corresponding to a fixed TOF bite, ΔT, is

$$\Delta P_p = \frac{EP_p^2}{Lm^2c^2}\Delta T. \tag{2.5}$$

Since iT_{11} contains only the ratio of cross sections, most factors cancel out, and only relative cross sections need to be determined:

$$\sigma = \frac{\text{Yield}}{N_{\text{beam}} \, \epsilon}. \tag{2.6}$$

The uncertainty in iT_{11} is determined from the weighted sum in quadrature of all of the contributing uncertainties, where the weighting is the partial derivative of the observable with respect to each quantity,

$$\begin{aligned}(diT_{11})^2 = &\left(\frac{\partial iT_{11}}{\partial\sigma_+}d\sigma_+\right)^2 + \left(\frac{\partial iT_{11}}{\partial\sigma_-}d\sigma_-\right)^2 \\ &+ \left(\frac{\partial iT_{11}}{\partial\sigma_b}d\sigma_b\right)^2 + \left(\frac{\partial iT_{11}}{\partial P_z^+}dP_z^+\right)^2 \\ &+ \left(\frac{\partial iT_{11}}{\partial P_z^-}dP_z^-\right)^2,\end{aligned} \tag{2.7}$$

where $d\sigma_+$, $d\sigma_-$, and $d\sigma_b$ are the statistical uncertainties in the measurements of the relative cross sections, and $dP_z^\pm$ is the uncertainty in the target polarization. The uncertainties of N_b, ϵ, and target thicknesses are negligible.

B. Targets

The TRIUMF polarized deuteron target has been described previously [9,10]. The target cell consisted of a rectangular box with 0.051 mm mylar walls and dimensions 17 mm $\times$18 mm $\times$5 mm. The cell was oriented so that the

normal to the downstream face made an angle of 10° to the right (from above) with the undeflected beam direction. The cell was filled with 1 mm diameter beads of deuterated butanol doped with {sodium bis[2-ethyl-2-hydroxybutanoato-(2-)]oxochromate-V} EHBA-Cr^{v} dissolved in D_2O. The cell was immersed in a mixture of $^3He/^4He$ in the mixing chamber of a dilution refrigerator. The polarizing field of 2.5 T was provided by a split pair of superconducting coils.

Dynamic polarization of the deuterons was achieved by irradiating the target beads with microwaves. The polarity of the target polarization was determined by selecting one of two independently supplied microwave frequencies. The magnitude of the target polarization was determined from measurements of the deuteron nuclear magnetic resonance (NMR) signal, which was calibrated using the thermal equilibrium (TE) technique. The NMR pickup coil was made of 0.1 mm diameter copper wire and was mounted inside the target cell. Three TE calibrations were made during the experiment. Polarizations $P^+ = 24.0\%$ and $P^- = 27.6\%$ were obtained during the 134 MeV data taking. Polarizations $P^+ = 25.6\%$ and $P^- = 32.4\%$ were obtained during the 228 MeV data taking.

The background target consisted of a rectangular carbon slab of dimensions 17.8 mm $\times$ 17.6 mm $\times$ 1.6 mm, chosen to simulate both the carbon and oxygen nuclei in the deuterated butanol. To account for the copper nuclei in the NMR coil, the carbon slab was wrapped in a copper foil of thickness 0.045 mm. This was then placed in a mylar sleeve equivalent to the walls of the foreground target cell. The amount of helium traversed by the beam was roughly equivalent between the foreground and background targets. The dimensions of the background target were chosen to match the energy loss characteristics of the foreground target, since the target magnetic field acts like a momentum analyzer. There were thus different numbers of carbon nuclei between the foreground and background targets. The background target was placed on a target ladder just below the foreground target. Either target could easily be moved into the beam without having to make other changes. Background events amounted to about 32% of the foreground, typically, in the region of quasifree kinematics.

In order to calibrate the TOF as a function of the momentum, a special calibration target was also used. This consisted of a rectangular slab of CH_2 of dimensions 26.0 mm $\times$ 31.5 mm $\times$ 3.6 mm. This target was placed in the cryostat, but without helium present. Its dimensions were also chosen to match the energy loss characteristics of the foreground target. The 2.5 T field pointed up in the lab, thus positively charged particles were deflected to the right looking downstream. The full deflection of unreacting beam pions varied from 19.7° at 228 MeV to 28.5° at 134 MeV.

C. Operating procedure

This experiment was run in the M11 medium energy (80–300 MeV) pion channel at TRIUMF. This channel produces a beam spot of approximately 1.6 cm in diameter at the focus. This was checked with a charge integrating wire chamber. The momentum resolution ($\Delta P_\pi / P_\pi$) of M11, defined by a set of horizontal slits, was 1%. Proton contamination in the incident beam was reduced by a differential degrader located

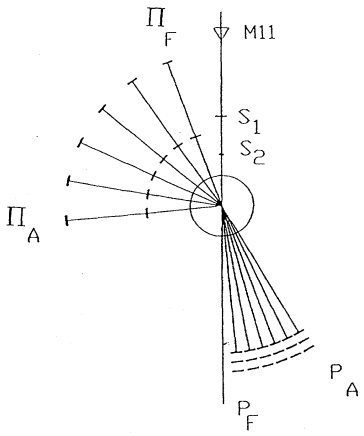

FIG. 1. The time-of-flight spectrometer arrangement in the medium energy pion channel M11.

at the channel midplane. A wall of lead bricks just to the left of the beam looking downstream served as a low energy proton dump.

For a specific incident particle energy, it is sufficient to observe and identify two of the three final-state particles at well defined angles, and to measure the momentum of one of them, in order to determine any of the kinematic variables for any of the reaction products, including the third (undetected) particle. This is the minimum requirement for kinematical completeness, which was achieved in this experiment by coincident detection of the pion and proton, in conjunction with a measure of the proton momentum from its TOF.

The detection system used for this experiment was a time-of-flight (TOF) spectrometer, Fig. 1, an arrangement of counters previously used in the study of πd elastic scattering [10]. The spectrometer consists of six pion telescopes and six complementary proton telescopes.

The pion telescopes were set up to the right of the beam looking downstream, covering the lab angles (i.e., with respect to the undeflected beam) 85° to 150° at 228 MeV, 95° to 155° at 134 MeV, and 90° to 155° at 180 MeV. The scattering angles of the particles with respect to the beam are of course different due to the deflections in the target magnetic field. A geometrical solid angle of 18.0 m sr for each of six independent arms ($i = 1,6$) was defined by a plastic scintillator, ($\Pi 2_i$), of dimensions 9.0$\times$31.0 cm^2 and 4.76 mm thick, located 124.5 cm from the polarized target. Both ends of the scintillator were viewed by photomultiplier tubes enabling good timing and pulse height resolution. This scintillator provided TOF and energy loss (ΔE) information. Together with another scintillator, ($\Pi 1_i$), of dimensions 9.0$\times$20.0 cm^2 and 3.18 mm thick, located at a radius of 74.0 cm, this constituted one of six pion telescopes. A pion arm event, "Π_i", consisted of $[(\Pi 2 \uparrow \Pi 2 \downarrow \mathrm{MT}) \cdot \Pi 1]_i$, where MT is the hardware meantime.

The six proton arms were set up to the left of the beam direction, covering the lab angles 4.0° to 28.8° at 228 MeV, $-0.2°$ to 21.7° at 134 MeV, and 1.4° to 24.9° at 180 MeV. Each proton arm consisted of three scintillators. The first scintillator, ($P1_i$), of dimensions 9.0$\times$40.0 cm^2 and 3.18

mm thick, was located at a radius of 129.2 cm, defining a solid angle of 21.6 m sr. Both ends of this scintillator were viewed by photomultiplier tubes. This scintillator provided the TOF information. Following this was a 12.7 mm thick scintillator, $(P2_i)$, of dimensions 9.0×41.0 cm^2 at a radius of 134.9 cm. The third scintillator, $(P3_i)$, of dimensions 9.0×41.0 cm^2 was 6.35 mm thick and located at a radius of 136.9 cm. Each scintillator provided energy loss information. A proton arm event, "P_i", consisted of $(P1\uparrow P1\downarrow \mathrm{MT})_i$. The signals $P2_i$ and $P3_i$ were not included in the coincidence because some of the protons from the breakup reaction do not have sufficient energy to pass through the first scintillator. Thresholds on the $(P1_i)$ were set below the proton signals, but mostly above the pion signals, serving to electronically eliminate most events with pions detected in the proton arms.

The twelve arms were arranged in a matrix configuration, with the smallest pion angle (π-arm A) through the largest (π-arm F) located at complementary angles to the largest proton angle (p-arm A) through to the smallest proton angle (p-arm F), such that the diagonal combinations (π-arm A in coincidence with p-arm A, etc.) of the angle matrix corresponded to the kinematics of the free πp elastic scattering reaction. The electronics trigger for the experiment was arranged such that each pion telescope was in coincidence with each of the proton telescopes, i.e., 36 πp angle pairs were recorded simultaneously.

The flux of the incident beam was counted directly with scintillators $S1$ (8.0×8.0 cm^2 and 3.18 mm thick) and $S2$ (3.0×1.4 cm^2 and 1.59 mm thick) in coincidence. $S1$ was located 86.2 cm and $S2$ 53.6 cm upstream of the target. The image of $S2$, which was mounted with its long side vertical, was smaller than the target itself. Residual protons in the beam were eliminated from the trigger and the beam scaler by placing an upper level threshold on the pulse height from $S2$. This $\overline{S2}$ threshold was set above the two pion signal, but below the proton signal. The beam coincidence, "B", was defined by $S1\cdot S2\cdot\overline{S2}$, yielding a rate of 1.6 MHz.

The event definition consisted of the coincidence between the incident beam counters and any πp coincidence, $B\cdot\Pi_i\cdot P_j$ $(i,j = 1,6)$. $S2$ defined the timing of the event presented to the computer, as well as the start timing of all the TDC's (time-to-digital convertors). The signals from $P1$, $\Pi2$, and $S2$, which defined the timing of the p-arm, π-arm, and beam coincidences, respectively, were passed through constant fraction discriminators.

The setup procedure was as follows. With the proton arms disabled, the π arms were placed individually in the beam and variable delays from each arm were adjusted so that the beam was correctly timed in at each event coincidence. All counters were then set at their complementary angles for free πp scattering. The proton arms were put back in the πp coincidence, but with only the diagonal coincidences enabled (π-arm A with p-arm A, etc.). Using the quasifree πp reaction from the deuterated butanol target, variable delays from each p arm were adjusted to time in the πp coincidences. This procedure served to synchronize the proton arms and to ensure that the π arm defined the timing for all 36 πp coincidences. The matrix of coincidences was thus timed in for all ranges of proton momentum of interest for each of the incident beam energies in the experiment. Finally, all 36 πp coincidences were enabled.

Data were obtained at three different π^+ beam energies: 6 044 000 events at 228 MeV, 5 885 000 events at 134 MeV, and 8 957 000 events at 180 MeV. After the data had been taken at 134 MeV, the CH_2 calibration target was inserted (with the field still on) for three calibration runs (at 134 MeV) making use of the free πp reaction. This procedure is described below. In order to check for systematic errors, blocks of data consisting of runs with the same polarization were obtained in the sequence:

$$\begin{aligned}
228\ \text{MeV:}&-1\ +1\quad B1\quad +2\ -2\\
&+3\ -3\ U1\ B2\ U2\ -4\ +4,\\
134\ \text{MeV:}&+1\ -1\ U1\ B1\ U2\ -2\ +2\\
&+3\ -3\ U3\ B2\ U4\ -4\ +4,\\
180\ \text{MeV:}&+1\ -1\ U1\ B1\ U2\ -2\ +2\\
&+3\ -3\ U3\ B2\ U4\ -4\ +4
\end{aligned}$$

(where "+1" is a label for the first block of positive polarized runs, "B" is for a block of runs with the background target, "U" is for unpolarized runs, etc.).

III. DATA ANALYSIS

A. Event-by-event analysis

The two-body final state of the πp reaction was simulated in a ray tracing program, incorporating the kinematics of the scattering, a map of the target magnetic field, and energy loss effects in the target cell and surrounding thermal shields. For a given angle pair coincidence, the momentum of the proton and of the pion were predicted and compared with the measured TOF of each particle for each angle pair, to give a conversion between TOF and momentum for that particle. Calibration points were obtained for a variety of momenta with each complementary pair of arms.

Three sets of synchronizing constants were extracted from the calibration runs, enabling the absolute TOF of a pion or proton to be determined, regardless of which angle pair generated the trigger. The first set of constants synchronizes the start time for any event, independent of which of the six event coincidences caused the computer interrupt. The other two sets of synchronization constants amounted to essentially fine adjustment of the variable hardware delays of the p and π arms, as discussed above. With all 18 constants in use, the absolute TOF calibration derived from the above two-body measurements was also appropriate for coincidences from the three-body final state, including angle pairs off the diagonal of the angle pair matrix. Relations between absolute TOF and particle momentum were also determined from these calibration runs.

A series of cuts was then applied to the data from the foreground target to screen out all but the reaction of interest, $\pi^+ d\rightarrow pn\pi^+$. The same cuts were then applied to the data from the background target.

In the first cut, data were required to fall inside a polygon in a two-dimensional (2D) plot of $(P1+P2+P3)$ analog-to-digital converter (ADC) versus $P1$-MT-TDC, to identify

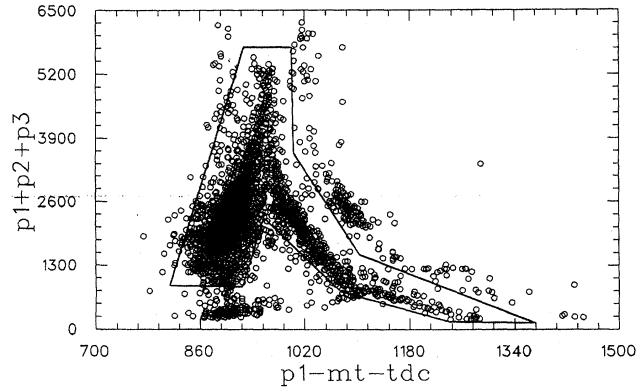

FIG. 2. Plot of normalized $(P1+P2+P3)$ ADC signal versus $P1$-MT-TDC signal, for p-arm F in coincidence with π-arm F, for an equal amount of data from a foreground run at each of the three energies. The polygon cut is indicated.

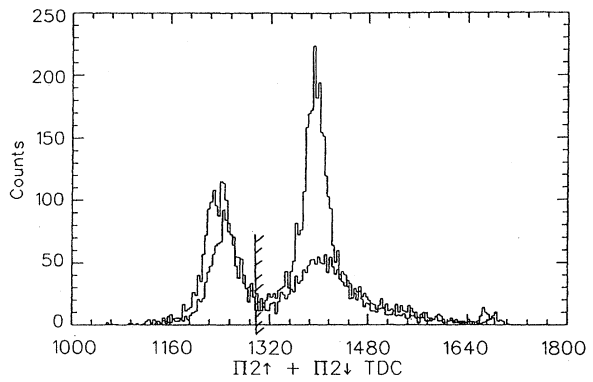

FIG. 3. Histogram of $(\Pi2\uparrow+\ \Pi2\downarrow)$ TDC signal for p-arm B in coincidence with π-arm E at 228 MeV with no cuts applied. A foreground run is shown superimposed on a background run. The cut on this quantity is indicated.

the particle type. A proton signal lies on a "passing band" at small TOF (high velocity) and a "stopping band" at larger TOF (low velocity). The deuteron "stopping band" is separated from, and lies above that of the proton. (Deuterons from πd elastic scattering do not have sufficient energy to pass through all three scintillators at the energies used in this experiment.) A polygon cut selecting the proton band therefore includes all protons passing the proton arm, may include some pions, but eliminates deuterons. Before this cut could be applied, the $P1$, $P2$, and $P3$ ADC gains were adjusted until a reasonable proton band was obtained, and the deuteron band could be distinguished. Six different polygon cuts were applied, one for each of the proton arms.

As an example, Fig. 2 shows this cut for p-arm F in coincidence with π-arm F, along with the polygon cut, with an equal amount of data included from foreground runs at each of the three energies. The band of dots below the polygon near 900 TDC units is due to particles which do not deposit their predicted amount of energy due to nuclear reactions within the scintillators. The factor ϵ_p in Eq. (2.4) corrects for these protons excluded from the analysis. It is noted that this factor cancels out in iT_{11}, as discussed above.

The second cut applied was to the sum of TDC signals from both ends of the Π2 detector to remove the absorption events, $\pi^+ d \rightarrow pp$. The data from 228 MeV are used as an example. A histogram of Π2-SUM-TDC for p-arm B in coincidence with π-arm E is shown for a foreground run in Fig. 3. An appropriately scaled background run is also shown below the foreground data as discussed below. The peak near 1225 TDC units is due to pions from $\pi^+ d \rightarrow pn\pi^+$ and the peak near 1385 TDC units is due to protons from $\pi^+ d \rightarrow pp$. The cut shown, therefore, eliminates the absorption events. From straightforward kinematics it can be shown that protons detected in the pion arm from absorption are faster than the deuterons from πd elastic scattering, and also faster than the protons from the breakup reaction. This cut, therefore, eliminates all absorption events and breakup events with the proton detected in the pion arm (a reversed event from those of interest). The use of a cut on the Π2-SUM-TDC signal removes some events of interest where the pion momentum falls below some "critical" value, which is a function of the cut applied. From kinematics, there is a corresponding "critical" proton momentum above which events are rejected, and this forms the upper limit for which results are quoted.

The ratio of target thicknesses was determined as follows. Consider, for example, Fig. 3. The Π2-SUM-TDC histogram, with no cuts applied, shows a $\pi d \rightarrow pn\pi$ peak, and a $\pi d \rightarrow pp$ peak at larger TOF. Since $\pi d \rightarrow pp$ is a two-body reaction, the peak is fairly narrow (i.e., at a particular TOF). The "tail" of this distribution at larger TOF is entirely due to quasifree scattering on background nuclei in the target. Figure 3 shows a background run superimposed on the foreground data. The background data were first scaled to account for the difference in N_{beam} and ϵ between the two runs. The additional factor required to make the two curves overlay at large TOF was then determined. A variety of different combinations of foreground and background runs for several different coincidences were examined.

B. Determination of iT_{11}

The quantity histogrammed to give the yield (from which the relative cross sections are calculated) was the proton TOF, $P1$-MT-TDC. The lower TOF limit corresponded to the critical proton momentum cutoff discussed above. A histogram bin consisted of 3 TDC channels, which is equivalent to 150 psec. Figure 4 shows a typical histogram for a foreground run and an appropriately scaled background run for p-arm A in coincidence with π-arm A at 228 MeV, with all cuts applied.

The results of the event-by-event analysis were compiled as 36 such histograms, one for each coincidence, for each run. These histograms served as input for a program to calculate iT_{11}, which was determined for each momentum bin for each of the 36 coincidences, yielding 36 tables of iT_{11} versus proton momentum. Eight histogram TOF bins were combined to make one momentum bin. Each momentum bin thus corresponded to a TOF bin of 1.2 nsec. From Eq. (2.5) this leads to a nonlinear momentum binning from about 10 MeV/c for 200 MeV/c protons to 80 MeV/c for 500 MeV/c protons.

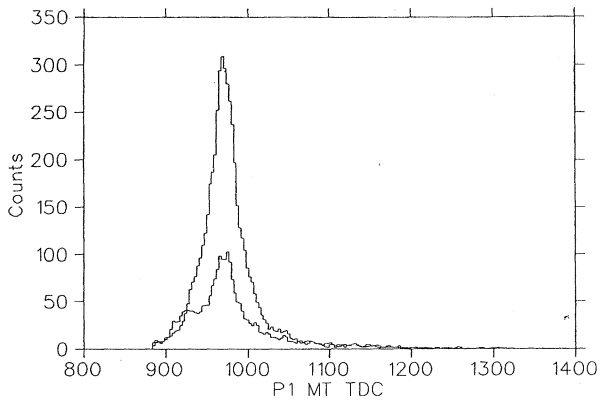

FIG. 4. Histogram of $P1$-MT-TDC signal for p-arm A in coincidence with π-arm A at 228 MeV. A foreground run (large peak) is shown superimposed on a background run. All cuts have been applied.

As can be seen in Fig. 4, the shape of the "Yield" curves is sharply peaked. Since iT_{11} is calculated on a (momentum) bin-by-bin basis, it is important to determine the sensitivity of the results to small shifts in the start-time signal, which would tend to displace one histogram relative to another. The coincidence p-arm B with π-arm B at 228 MeV is used as an example of this sensitivity. If we enter a single run as a "+" run in the iT_{11} program, and also as if it were a "−" run (in the manner used for the systematic checks described below) we obtain a result identically zero. This particular run was then reanalyzed with the event-by-event program, except this time a constant shift of +3.0 TDC channels (one histogram bin) was added to the $P1$-MT-TDC signal. The unshifted data were now entered as a "+" run in the iT_{11} program, and the shifted data as a "−" run. The resulting asymmetry is shown in Fig. 5. This asymmetry plot has the same scales as the final iT_{11} results. Clearly a timing shift equivalent to only one histogram bin can have a dramatic effect on iT_{11}. Our data from all three energies appeared to have such a start-time shift occurring from run to run. This observation was based on a lack of self-consistency when the systematic

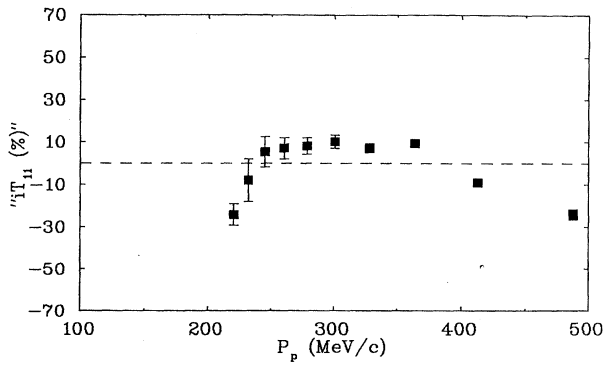

FIG. 5. Plot of "iT_{11}" versus P_p (MeV/c) showing the effect of a 3 TDC channel timing shift in the $P1$-MT-TDC signal. The construction of this plot is described in the text.

checks were applied, and the appearance of the characteristic shape of Fig. 5 in regions where the iT_{11} curve was expected to be flat.

To account for this start-time shift, a run-dependent correction was determined, based on the shift required to stabilize a well defined quantity known to be constant for a given energy; namely, the TOF of a beam particle between the $S1$ and $S2$ scintillators. These small run-dependent shifts (typically less than one histogram bin width) were inserted in the event-by-event program, and the entire data set reanalyzed.

C. Systematic checks and final calculation

The self-consistency of the data was checked, to reveal any systematic problems, in the following manner. Consider all the "+" data obtained at a particular energy as an example. This was all entered as "+" data in the iT_{11} program. Then the data from one of these "+" runs was entered as if it were a "−" run. Barring any systematic problems, the resulting asymmetry should give a result consistent with zero. A χ^2 test was used in comparing the asymmetry results with zero for all bins of all 36 histograms. Each run was compared individually against the combination of all others with the same polarization in the same manner.

Next, each block of "+" data was compared against the sum of the remaining "+" blocks; e.g., +2, +3, and +4 were all entered as "+" data, and +1 was entered as "−" data. Finally, "systematic plots" of the "+" data were made by entering half of the blocks, e.g., +1 and +4, as "+" data and half, +2 and +3, as "−" data. This procedure was then repeated for the true "−" data at this energy, then for the other two energies.

It was found that in general each block of "+" and "−" data was internally consistent (i.e., no one run compared to the total had a χ^2 significantly different from any of the others, with the exception of one run in the −4 block at 180 MeV). It was also found that omitting complete blocks which contributed values of χ^2 significantly larger than the other blocks led to an improvement in the consistency of the remaining blocks as evidenced by the systematic plots. A separate systematic plot was examined for each of the 36 coincidences. This procedure was iterated several times, until self-consistency was obtained, with the following blocks omitted from the final results: 228 MeV: −1; 134 MeV: −4, +4; 180 MeV +1, −3. A systematic plot for the "+" and "−" data at 134 MeV, p-arm C in coincidence with π-arm C, is shown in Fig. 6 as an example.

It is suspected that the problem in the omitted blocks of data is caused by some small timing shift in addition to the run-dependent shifts already corrected for in the event by event analysis. Note that it is the shift of one block relative to another that is important, rather than the small absolute shifts. At 228 MeV, the first block is the only one omitted. The remaining "+" blocks are consistent with each other, as are the "−" blocks. The same argument can be made for the 134 MeV data, where the last two blocks were omitted. However, the same argument cannot be made at 180 MeV, since the remaining blocks are not consecutive. If we ignore this fact, and calculate iT_{11} anyway, the results show the characteristic shape of a timing shift in regions where iT_{11} is expected to be flat. This confirms our lack of confidence in

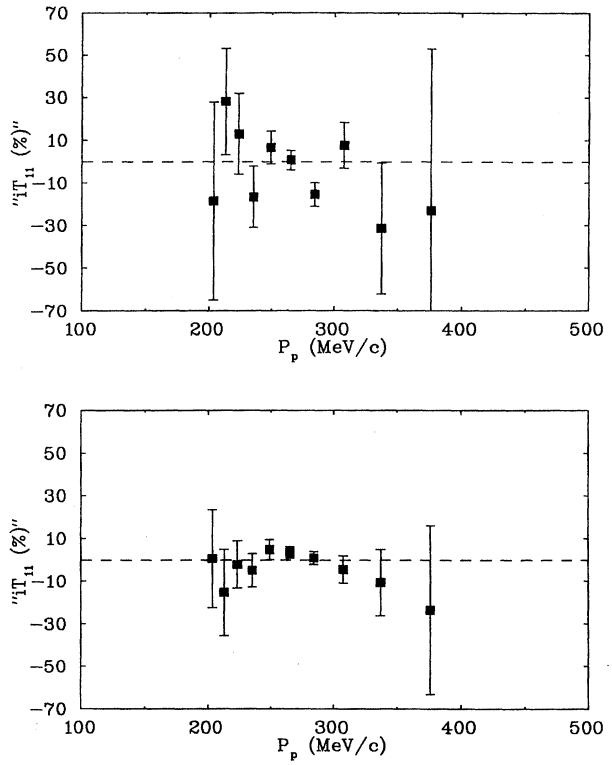

FIG. 6. Plots of the systematic checks on the 134 MeV data, p-arm C in coincidence with π-arm C: (a) "+" data; (b) "−" data.

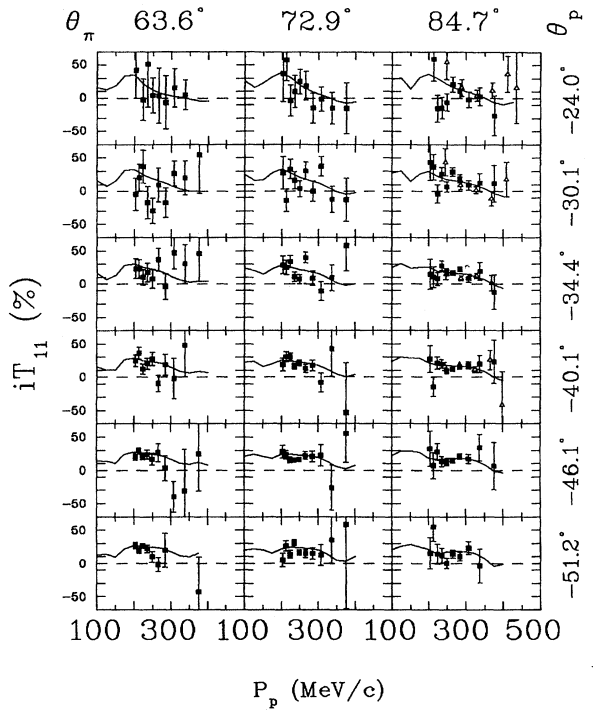

FIG. 7. Plots of iT_{11} (%) versus outgoing proton momentum P_p (MeV/c) for 18 πp angle pair coincidences at 134 MeV. The angle labels are described in the text. △: List *et al.*; □: This work. The curves are predictions of a relativistic Faddeev calculation by Garcilazo (AAY theory).

the 180 MeV data set and results for this energy are thus not reported. Note that the 180 MeV data set was obtained at the end of the running period, and further systematic tests were not possible in the remaining time available. Final iT_{11} results were calculated for all 36 coincidences at 228 and 134 MeV, omitting the indicated blocks.

IV. RESULTS AND DISCUSSION

For brevity, tables of results are not included in this publication, but are available from the authors. Figures 7 and 8 show iT_{11} versus outgoing proton momentum, P_p, for the 36 angle pair coincidences at 134 MeV. Figures 9 and 10 show the 36 corresponding plots at 228 MeV. The plots lying on the diagonal from bottom left in Figs. 7 and 9 to top right in Figures 8 and 10 correspond to the complementary angle pairs for free πp scattering. Each of these diagonal plots is labeled by a proton angle and a pion angle. These are the kinematical angles of the respective particles, i.e., measured with respect to the (deflected) beam at the target center, prior to being deflected by the target field on the way out. These angles are used to label the other coincidences.

Due to the momentum analyzing effect of the target magnetic field, each datum corresponds to a pion and proton angle which may differ by a few degrees from the mean angles labeling the plot. To compare with theory, iT_{11} was calculated point by point for the individual slightly varying angle pairs, although Gyles *et al.* showed that there was no significant difference between iT_{11} calculated in this manner or by using just the mean angles [11]. The solid lines are the predictions of a relativistic Faddeev calculation by Garcilazo based on the theory of Aaron, Amado, and Young (AAY) [6]. Also shown, where there is overlap, are the data of the Karlsruhe/SIN group [11,12]. In those regions of overlap with the previous measurements there is excellent agreement; confirming the results of List *et al.* at 134 MeV [12], and of Gyles *et al.* and List *et al.* at 228 MeV [11,12]. The agreement between these results, and those of the Karlsruhe/SIN group obtained with lower polarizations ($P_z^+ = 17.5\%$, $P_z^- = 20.0\%$ for Gyles *et al.*; $P_z^+ = 14.5\%$, $P_z^- = 15.3\%$ for List *et al.*), is another indication that the factor "X" in Eq. (2.1) is negligible. Data are presented for seven new angle pairs at 228 MeV and 20 new angle pairs at 134 MeV.

The theoretical iT_{11} results (AAY) are typically positive at low P_p, somewhat smaller and generally positive in the central P_p region, then finally crossing over to negative values at higher P_p. At 134 MeV, the predicted iT_{11} is smaller (in magnitude) than at 228 MeV, with less structure and a small angular variation. At both energies, there is generally excellent agreement between the theory and the data, in particular at the kinematics of QF scattering (typically the central P_p region). The predicted crossover to negative values at high P_p cannot be unambiguously confirmed, but the data are not inconsistent with this prediction.

In the QF region, the full Faddeev calculations of Garcilazo agree with the impulse approximation, but *overpredict* the (regular) breakup cross-section data by 30–40 % [5,6]. On the other hand, in the charge-exchange breakup reaction,

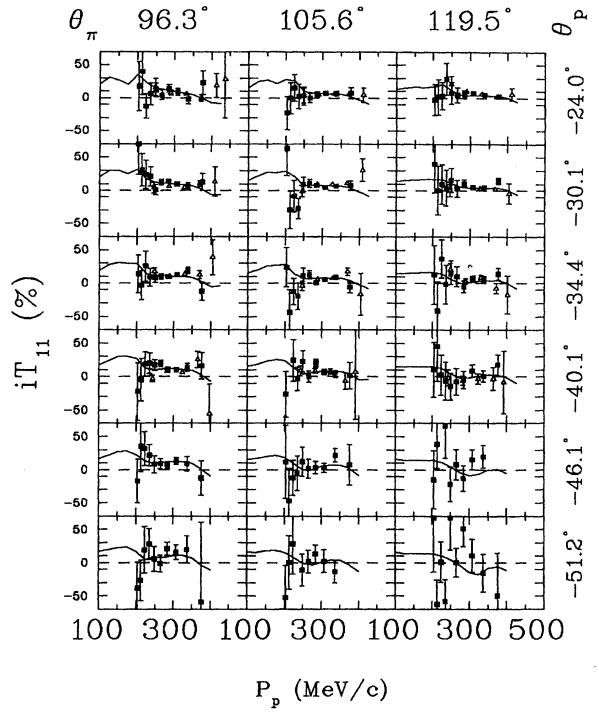

FIG. 8. Plots of iT_{11} (%) versus outgoing proton momentum P_p (MeV/c) for 18 πp angle pair coincidences at 134 MeV. The angle labels are described in the text. △: List *et al.*; □: This work. The curves are predictions of a relativistic Faddeev calculation by Garcilazo (AAY theory).

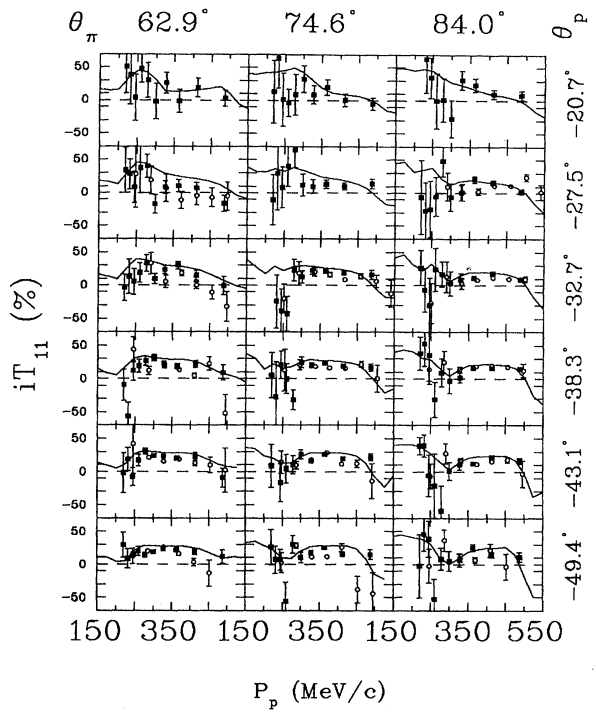

FIG. 9. Plots of iT_{11} (%) versus outgoing proton momentum P_p (MeV/c) for 18 πp angle pair coincidences at 228 MeV. The angle labels are described in the text. ⊙: Gyles *et al.*; □: This work. The curves are predictions of a relativistic Faddeev calculation by Garcilazo (AAY theory).

$\pi^+ d \to \pi^0 pp$ [13], the full calculation and impulse approximation agree with each other, but significantly *underpredict* the cross section data. By contrast, in comparing the measured and predicted iT_{11} in the QF region, the full calculations and impulse approximation all agree with each other, and with the data. Furthermore, the breakup reaction iT_{11} are consistent with A_y from free πp scattering [11,12]. A possible reason for this is that, because iT_{11} is a ratio of cross sections, the problems in the theoretical description of the cross sections have explicitly cancelled out.

At 228 MeV, the FSI region generally occurs at low P_p for forward θ_p and backward θ_π − see the top twelve plots in Fig. 10. Although the error bars in any one data set in this region make it difficult to draw a definitive conclusion, the combined results of the three independent measurements appear to indicate that the FSI are overpredicted somewhat in six of the twelve plots.

The "bumplike" structure predicted at high P_p in the lower plots of Fig. 10 is probably due to the formation of a Δ^{++}. Note that this is more evident in iT_{11} than in cross-section predictions. Unfortunately, the large structure predicted in iT_{11} away from the QF diagonal cannot be unambiguously confirmed.

Considering all of the measurements to date in the breakup channel, it is clear that the cross sections are not well described by the theory, whereas there is generally good agreement with iT_{11}, which by its nature is expected to be the more sensitive observable.

V. SUMMARY AND CONCLUSIONS

Results of iT_{11} versus outgoing proton momentum, P_p, are presented for 36 πp angle pair coincidences in the range $20.7° \leq \theta_p \leq 49.4°$, $62.9° \leq \theta_\pi \leq 123.7°$ at 228 MeV, and $24.0° \leq \theta_p \leq 51.2°$, $63.6° \leq \theta_\pi \leq 119.5°$ at 134 MeV. Results are presented for 7 new angle pairs and 29 overlapping angle pairs at 228 MeV; and 20 new angle pairs and 16 overlapping angle pairs at 134 MeV.

The results are compared with the predictions of Garcilazo based on the Aaron, Amado, and Young (AAY) theory. At both energies there is generally excellent agreement between theoretical and measured iT_{11}, in particular at the kinematics of QF scattering. In all regions of overlap with the previous measurements of the Karlsruhe-SIN group there is excellent agreement between the experiments.

There are two specific areas where the comparison between theory and data is less satisfactory.

At 228 MeV, the FSI are overpredicted somewhat in 6 of the 12 plots where FSI are expected to be significant. If this is correct, then the $J^p = 2^+$ state (where the Δ and nucleon are in a relative S state with their spins parallel) which gives rise to the triplet NN FSI is not as dominant in the πd system as is presently thought [14]. This should be tested in an experiment measuring iT_{11} exclusively in the np FSI region.

In the QF region, the theory and previously measured cross-section data disagree by up to 40% for some coincidences, whereas iT_{11} is well described and agrees with data

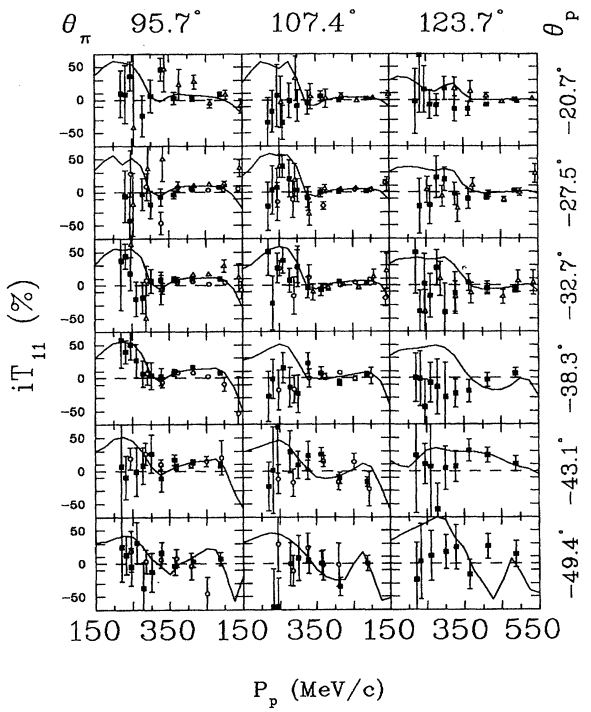

FIG. 10. Plots of iT_{11} (%) versus outgoing proton momentum P_p (MeV/c) for 18 πp angle pair coincidences at 228 MeV. The angle labels are described in the text. △: List *et al.*; ⊙: Gyles *et al.*; □: This work. The curves are predictions of a relativistic Faddeev calculation by Garcilazo (AAY theory).

from free πp scattering. A possible reason for this is that because iT_{11} is a ratio of cross sections, the problems in the theoretical description of the cross-sections have cancelled out. The cross-section problem may also indicate that some dynamic effect is at work, which is not treated in the present theory. Such a process is required to give the "spectator" nucleon a large momentum (compared to its Fermi momentum) with much greater probability than in the current models. A direct interaction between the Δ and the nucleon may be able to supply the required momentum. Another suggestion invokes a three-body force by which the incident pion interacts with the whole deuteron instead of just one of the constituents [5].

The effects of including a direct interaction between the Δ and the nucleon, and of a three-body force should be investigated theoretically. To date, only Garcilazo has provided calculations for the three-body final state. Independent calculations from other theory groups would be valuable. It would be useful to express the breakup reaction observables in terms of, for example, helicity amplitudes, to see which amplitude could have a large effect on the cross section, but a small effect on iT_{11}. Also, in the charge-exchange breakup reaction the dominant $^3S_1$ NN FSI is forbidden by the Pauli exclusion principle so that only the weak $^1S_0$ FSI enters. This reaction may, therefore, be well suited to study of the quasi-two-body reactions $\pi^+ d \rightarrow p\Delta^+$ and $\pi^- d \rightarrow n\Delta^0$, in order to isolate effects of the ΔN interaction [13].

To continue the process of improving the data base of complementary observables, the following two measurements are suggested.

(i) iT_{11} in the charge-exchange breakup reaction: Theoretical predictions show distinct structure and sizable values in some regions of phase space [13].

(ii) T_{20} (tensor analyzing power) in the normal breakup reaction: Theoretical predictions show T_{20} to exhibit considerable structure with strong sensitivity to np FSI [11].

However, both of these experiments measure observables containing ratios of cross sections which, as mentioned above, may be masking problems. Independent measurements of cross sections should also be made with a magnetic device to verify the results from TOF measurements.

ACKNOWLEDGMENTS

We gratefully acknowledge the contributions of the TRIUMF technical, offline computing and operations staffs, as well as financial support from the Natural Sciences and Engineering Research Council of Canada.

[1] W. Kluge, Rep. Prog. Phys. **54**, 1251 (1991).
[2] J. M. Eisenberg and D. S. Koltun, *Theory of Meson Interactions with Nuclei* (John Wiley and Sons, New York, 1980).
[3] T. Ericson and W. Weise, *Pions and Nuclei* (Clarendon Press, Oxford, 1988).
[4] H. Garcilazo and T. Mizutani, *πNN Systems* (World Scientific, Singapore, 1990).
[5] P. V. Pancella *et al.*, Phys. Rev. C **38**, 2716 (1988).
[6] E. L. Mathie *et al.*, Phys. Rev. C **41**, 193 (1990).
[7] D. M. Yeomans *et al.*, Phys. Rev. C **49**, 2898 (1994).
[8] *Proceedings of the Third International Symposium on Polarization Phenomena in Nuclear Reactions*, edited by H. H. Barschall and W. Haeberli, University of Wisconsin, Madison, 1970.
[9] G. R. Smith *et al.*, Nucl. Instrum. Methods A **254**, 263 (1987).
[10] G. R. Smith *et al.*, Phys. Rev. C **38**, 251 (1988).
[11] W. Gyles *et al.*, Phys. Rev. C **33**, 595 (1986).
[12] W. List *et al.*, Phys. Rev. C **37**, 1594 (1988).
[13] R. Tacik *et al.*, Phys. Rev. C **42**, 1846 (1990).
[14] W. List *et al.*, Phys. Rev. C **37**, 1587 (1988).